Submitted to Shape Memory and Superelasticity in October 2018

Pathways towards grain boundary engineering for improved structural performance in polycrystalline Co-Ni-Ga shape memory alloys

C. Lauhoff[1], M. Vollmer[1], P. Krooß[1*], I. Kireeva[2], Y.I. Chumlyakov[2], T. Niendorf[1]

[1]*Institut für Werkstofftechnik (Materials Engineering), Universität Kassel, 34125 Kassel, Germany*
[2]*Siberian Physical Technical Institute, Tomsk State University, Novosobornay Square 1, 634050 Tomsk, Russia*

Abstract

Co-Ni-Ga high-temperature shape memory alloys attracted a lot of scientific attention due to their superior functional material properties in recent years. In the single crystalline state Co-Ni-Ga HT-SMAs feature a good pseudoelastic response up to 500°C. However, in the polycrystalline condition Co-Ni-Ga suffers significant grain constraints and premature fracture at grain boundaries. In this regard, crystallographic orientation of the grain being involved as well as morphology and geometrical orientation of the grain boundaries with respect to the loading direction under pseudoelastic deformation is expected to be of crucial importance. Therefore, this study addresses the structural integrity of engineered grain boundaries, i.e. specifically selected grain boundaries in terms of orientation, grain boundary morphology and crystallographic grain orientation of adjacent grains. Mechanical testing combined with *in situ* methods and *post mortem* scanning electron microscopy investigations are used to shed light on the prevailing microstructural features resulting in any kind of structural degradation.

Keywords: High-temperature shape memory alloys (HT-SMAs), grain boundary, grain boundary engineering, structural degradation, Co-Ni-Ga

*Corresponding author: E-mail address: krooss@uni-kassel.de

Introduction

Over the last decades shape memory alloys (SMAs) have gained increasing interest owing to their unique functional properties, which are based on a thermoelastic, fully reversible phase transformation between a high-temperature austenitic phase and low-temperature martensitic phase. Large reversible strains up to about 10 % and high damping capacity qualify SMAs as promising materials for applications as solid state actuators and damping devices [1,2]. However, in order to overcome the limitations of conventional binary Ni-Ti SMAs, i.e. to allow for application temperatures above 80°C, efforts in industry and academia have been made to introduce new alloy systems featuring increased martensite start temperatures (M_s), referred to as high-temperature (HT-) SMAs. Thereby, applications at higher operating temperatures become feasible in the fields of aerospace, automotive and the energy sector, where application temperatures often exceed 100°C [3,4]. Cu-based, Ti-Ta-based, Ni-Al-based and Ni-Ti-based have been proposed as potential HT-SMA candidates. However, several drawbacks ranging from thermal instabilities due to decomposition processes, limited workability due to pronounced brittleness and poor functional fatigue properties still hinder their widespread use in industrial application [3–5]. Up to now, Ni-Ti-X alloys with high amounts of noble and refractory elements (X) are the most promising HT-SMA candidates. However, these alloys suffer high cost of some of the constituent elements as well as pronounced brittleness [4,6].

Heusler-type Co-Ni-Ga alloys, whose development was guided by research on the intensively studied Ni-Al binary system [2], have received considerable attention as an attractive alternative to overcome these issues: Co-Ni-Ga undergoes a martensitic transformation from a cubic B2-ordered austenite to a tetragonal $L1_0$ martensite [7]. Relatively inexpensive alloying elements as well as improved workability due to the potential segregation of the ductile disordered

secondary A1 γ-phase are beneficial for any envisaged industrial application [8]. The fundamental properties of this alloy system such as structural and phase transformation characteristics [7–10] as well as shape memory and pseudoelastic behavior (i.e. transformation temperatures and strains, thermal and mechanical hysteresis and cyclic stability as a function of temperature, stress state and nanometric particles) [11–17] have been comprehensively reported in literature. Particularly, the fully reversible pseudoelastic response in a large temperature range up to 500°C [11,12,18] and perfect cyclic stability without any kind of functional degradation up to 100°C [16,17] makes Co-Ni-Ga very attractive for high-temperature damping applications.

For most of the envisaged applications polycrystalline material is crucially needed. Due to limited producibility and increased manufacturing costs, single crystalline material is not attractive for industrial application. However, the majority of research focused on Co-Ni-Ga single crystals, primarily, with ⟨001⟩ orientation [4]. Only a limited number of studies are available in literature detailing mechanical functional properties of polycrystalline material [8,19]. As this alloy system is characterized by a pronounced orientation dependence of transformation strains in compression and tension [17], polycrystalline structures suffer from pronounced deformation constraints. These constraints cannot be sufficiently accommodated owing to a limited number of martensite variants during the cubic ⇌ tetragonal martensite transformation in Co-Ni-Ga. As a consequence, geometrical incompatibilities at the grain boundaries result in high stresses leading to intergranular fracture, being the dominant failure mechanism upon mechanical loading [4]. Consequently, polycrystalline Co-Ni-Ga HT-SMAs with random grain orientation show poor functional performance eventually hindering their wide spread application.

In order to avoid intergranular fracture, precipitation of a ductile secondary phase along grain boundaries has been discussed and implemented in various SMAs [20–23]. Thereby transformation ductility is improved in these systems, since extensive plastic deformation of the secondary phase during loading helps to accommodate the transformation induced shape change of the matrix and can, thus, hinder intergranular crack nucleation and propagation [20]. However, deformation by dislocation slip and the volume fraction of the non-transforming secondary phases deteriorate shape memory reversibility and reduce transformation strains, respectively [8]. It was shown by Ueland and Schuh [24–26] that the pseudoelastic behavior of polycrystalline Cu-Zn-Al and Cu-Al-Ni samples suffer from large grain boundary (GB) areas and GB triple junctions. Due to the highly anisotropic transformation strains in these SMAs, pronounced incompatibilities lead to stress concentrations in the vicinity of GB triple junctions resulting in a complex multi-variant martensite morphology and concomitant rapid crack formation. In contrast, enhanced pseudoelastic properties were found in oligocrystalline structures, also referred to as bamboo structures, since GB areas were minimized and GB triple junctions were avoided. The improvement of the pseudoelastic behavior for microstructural conditions characterized by relative grain sizes exceeding the cross section of the samples was also shown in other SMAs, e.g. in Cu-Al-Mn [27–31] and Fe-Mn-Al-Ni(-Ti) [23,32–35]. Moreover, it was found in Co-Ni-Ga that a bamboo structured bicrystal showed a superior pseudoelastic response without crack formation and an improved functional fatigue behavior compared to reference polycrystalline samples [19]. However, up to now studies investigating the influence of the morphology of grain boundaries as well as the influence of the orientation of neighboring grains in oligocrystalline structures are still lacking. Recently, Liu et al. [36,37] found that an almost perfect pseudoelastic behavior can also be obtained in a condition featuring

solely columnar grains in a Cu-Al-Mn SMA with a strong ⟨001⟩ texture and geometrically absolutely straight low-energy grain boundaries. It can be assumed that the good pseudoelastic properties in this study are strongly influenced by the combination of the very low misorientation of neighboring grains and the very sophisticated GB morphology.

In order to investigate the role of specially selected grain orientations in combination with the morphology and orientation of correlated grain boundaries for highly anisotropic Co-Ni-Ga more systematically, different types of oligocrystalline compression samples were tested by means of *in situ* incremental strain tests. *Post mortem* scanning electron microscopy analysis using electron backscatter diffraction technique was conducted to establish interrelationships between microstructural features and structural as well as functional degradation upon pseudoelastic loading. In this regard, the present study focuses on damage tolerance, i.e. resistance against GB cracking. The beneficial effect of grain boundary engineering via ductile γ-phase precipitation will be detailed, whereas its deteriorating effects on the functional properties will be illustrated as well.

Materials and experimental techniques

Co-21%Ni-30%Ga (at.-%) ingots were produced by vacuum induction melting and the Bridgeman method was used to obtain a tricrystalline structure. Afterwards, compression samples with dimensions of 3 × 3 × 6 mm^3 and 4 × 4 × 8 mm^3 were wire-cut by electrical discharge machining (EDM) in a way such that each sample consisted of two or three grains separated by different kinds of grain boundaries. Samples were ground down to 5 µm grid size to remove the EDM affected surface layer and vibration-polished for 3h using a colloidal SiO_2 suspension with 0.02 µm particle size. A scanning electron microscope (SEM) operated at 20

kV equipped with an electron backscatter diffraction (EBSD) system was used in order to characterize the grain orientations as well as GB morphology. Samples were sealed into quartz tubes under argon atmosphere for further heat treatments. In order to exclude any effects of previous processing, samples were solution-annealed at 1200°C for 12h. Without quenching samples were then directly transferred to another furnace at 900°C for 4h in order to form ductile γ-phase at the GBs, followed by air cooling. Finally, a heat treatment at 300°C for 8.5h was conducted to enable pseudoelastic properties at ambient temperature [38] and samples were again ground down to 5 µm grid size.

Quasi-static uniaxial *in situ* incremental strain tests (IST) accompanied by optical microscopy (OM) were conducted at ambient temperature on a servo-hydraulic testing machine equipped with a Keyence digital microscope and the telezoom objective Z-100. The tests were carried out in displacement control at a nominal strain rate of 1×10^{-3} s^{-1}. Strains were measured using an extensometer with a gauge length of 12 mm. The ceramic rods were directly attached to the grips, which were treated as absolutely rigid for calculation of the nominal strain. In order to investigate the structural degradation under pseudoelastic loading, surface images were taken with a focus on the GB areas. Images were recorded at the maximum strain and after subsequent unloading to -100 N in each cycle employing pre-defined strain intervals. In addition to the standard silicon carbide grinding, the analyzed surfaces previously investigated via EBSD method for characterization of the GB characteristics were vibration-polished for 0.5h before testing. After mechanical testing, samples were again ground down and vibration-polished for *post mortem* EBSD.

Results and Discussion

In order to evaluate the structural degradation of the investigated Co-Ni-Ga material, i.e. formation of defects, as a function of grain misorientation and GB characteristics such as morphology and orientation with respect to the loading direction, compression ISTs at ambient temperature were conducted for bi- and tri-crystalline specimens. During each cycle *in situ* surface images in the loaded and unloaded condition were taken to reveal elementary microstructural processes and follow degradation at the GBs. Table 1 lists characteristics of the specimens investigated within this study.

Triple junction

Fig. 1 shows the pseudoelastic behavior and representative optical micrographs of a tri-crystalline specimen. As can be seen from the color coded orientation map of the entire sample and the color coding indicated in the standard triangle (cf. insets in the upper left and lower right part of the stress-strain diagram in Fig. 1, respectively) a GB triple junction is present separating three grains. Crystallographic orientations were found to be ⟨115⟩, ⟨103⟩ and ⟨112⟩ with respect to the loading direction (LD), which is highlighted by the black double arrow underneath the orientation map. Upon loading, the stress-induced martensitic transformation (SIMT) proceeds in a sequential manner. Due to the lower critical stress σ_{crit} for SIMT [39,40] in near ⟨001⟩ orientations, the SIMT starts within the ⟨115⟩ grain as it is shown in Fig. 1a. It is well known from literature, that many SMA systems, Co-Ni-Ga alloys [17,39,40] being a representative of this group, feature a pronounced orientation dependence of both σ_{crit} for SIMT and transformation strain. For the present grain orientations of the sample characterized in Fig. 1, theoretical calculations [17] and experimental results [39,40] for the single crystalline state under uniaxial loading reveal the lowest and highest value of σ_{crit} for the ⟨115⟩ and ⟨112⟩

orientation, and maximum theoretical transformation strains of -4.2 %, -4.2 % and -1.8 % for the ⟨115⟩, ⟨103⟩ and ⟨112⟩ orientation, respectively.

Due to the high transformation anisotropy, pronounced topography changes can be seen on the sample surface already at low strains, i.e. in the very early stages of the SIMT. These changes in topography are highly pronounced at the triple junction and the GB between the ⟨115⟩ and ⟨112⟩ grain. Further deformation results in a complete transformation of both grains accompanied by further increase of the surface topography. In consequence, surface regions in direct vicinity of the GBs are significantly distorted, and thus, appear dark in the optical micrographs shown in (a) and (b) (Fig. 1). After unloading from the maximum strain level of -4 %, substantial crack formation can be observed in this localized area. The corresponding micrograph (c) (Fig. 1) highlights premature failure of the specimen as a consequence of intergranular as well as transgranular fracture while (d) reveals traces of irreversible transformation in direct vicinity of the crack.

Based on *in situ* experiments and finite element calculations Ueland and Schuh [24] proved the detrimental effect of GB triple junctions on the damage evolution in micron-sized Cu-Zn-Al SMA wires. In addition, Vollmer et al. [19] supported these findings based on results obtained for the mechanical behavior of bulk polycrystalline Co-Ni-Ga. Owing to the large anisotropy of transformation strains, geometrical incompatibilities create high transformation-induced stress concentrations at the triple junction [24]. The *post mortem* EBSD image quality (IQ) map in Fig. 1d shows the evolution of several martensite plates (dark contrasted areas, due to the distorted nature of martensite) in the individual grains. Even this complex multi-variant martensite morphology as a result of the anisotropic transformation behavior and the irregular stress fields around the triple junction is not sufficient to accommodate the pronounced strain

incompatibilities [4]. This lack of accommodation is the key for rationalizing differences between single crystalline and polycrystalline Co-Ni-Ga: Single crystalline Co-Ni-Ga shows excellent functional properties and cyclic stability without any kind of functional and structural degradation up to 100°C [11,12,16]. The polycrystalline counterparts often suffer from premature fracture and show significantly reduced functional performance [19].

Bamboo grain structure

Fig. 2 shows the characteristic stress-strain curves of two bi-crystalline Co-Ni-Ga specimens. The EBSD orientation maps presented as insets in Fig. 2a and b reveal a single GB for each specimen exceeding the entire cross section and being almost perpendicular to the loading axis, i.e. a typical bamboo-like microstructure. Consequently, both specimens shown in Fig. 2 consist of two large grains. The values of maximum theoretical transformation strains in compression reported by Dadda et al. [17] are about -4.2 % for both, the ⟨105⟩ and ⟨115⟩ orientation, as well as -1.8 % and -4.0 % for the ⟨112⟩ and ⟨314⟩ orientation, respectively. Each of these grain-pairs feature different degrees of strain incompatibility, i.e. the difference between the maximum theoretical transformation strains ($\Delta\varepsilon_{theo}$). Whereas the combination of a ⟨105⟩- and ⟨314⟩-oriented grain in Fig. 2a results in 0.2 % total strain difference, the ⟨112⟩ and ⟨115⟩ pair encounters 2.4 % strain difference. Note, that the maximum theoretical transformation strain includes correspondent variant pair (CVP) formation strain and detwinning strain. Detwinning probably occurs in the last stage of deformation. However, since structural degradation also occurs at higher strains in this study, it is reasonable to compare maximum strain values.

Fig. 2 illustrates the stress-strain curves of both specimens highlighting significant differences regarding their functional properties in terms of the SIMT behavior and functional degradation.

Note that due to a considerable amount of irreversible strain after unloading from -3 % strain the IST in Fig. 2b was interrupted. Following a SEM analysis to investigate the underlying microstructural mechanism the IST was continued. The bi-crystal, which is characterized by the lower $\Delta\varepsilon_{theo}$ (Fig. 2a), features a continuous and smooth strain-hardening during the complete martensitic forward transformation. In contrast, a two-stage martensitic transformation is visible (Fig. 2b) upon loading for the specimen with a high $\Delta\varepsilon_{theo}$. In addition, both specimens reveal an accumulation of irreversible strain with increased applied compressive strain. After unloading from the maximum strain value of -6 % the amount of irreversible strain differs by a factor of about 2, i.e. 1.1 % and 2.0 % for the specimen with the lower and higher $\Delta\varepsilon_{theo}$, respectively. However, a quantitative evaluation of the extent of the irreversible strain accumulation is not reliable at this point. The different volume fractions of the ⟨105⟩- and ⟨115⟩-oriented grains (cf. Fig. 2), featuring nearly the same transformation characteristics, hinders a quantitative evaluation of functional degradation. In fact, only the qualitative investigation of structural degradation is in focus of the present study, quantitative analysis will be subject of future work.

Optical micrographs of the bamboo-like specimens recorded under load at various stages of the pseudoelastic stress-strain curves (Fig. 2) are shown in Fig. 3. Both grains of the bi-crystal with the lower $\Delta\varepsilon_{theo}$ (Fig. 2a), i.e. the ⟨105⟩- as well as the ⟨314⟩-oriented grain, reveal stress-induced martensite variants already at the very beginning of the martensitic transformation as evidenced by the micrograph at -2 % strain presented in Fig. 3b. In contrast, the SIMT exclusively starts in the ⟨115⟩-oriented grain of the specimen with the higher $\Delta\varepsilon_{theo}$ (cf. Fig. 3f at -1 % applied strain) until the martensitic transformation sets in in the neighboring ⟨112⟩-oriented grain at -2 % applied strain (cf. Fig. 3g). This sequential martensitic transformation is a good rationale for

the observed two-stage transformation behavior in Fig. 2b. Results are in good agreement with the data reported in Ref. [39,40]. According to data presented in those studies the near ⟨001⟩ and ⟨314⟩ crystallographic orientations have a similar, low resistance to martensitic transformation, whereas ⟨112⟩ is more unfavorable. Note the higher magnification of the micrographs in Fig. 3b and c highlighting the substantially different, i.e. smaller, dimensions of the martensite plates in the sample with a low $\Delta\varepsilon_{theo}$ compared to the sample with high $\Delta\varepsilon_{theo}$. Work on the morphology of stress-induced martensite and martensite variant selection during accommodation processes in differing microstructural conditions is currently in progress and will be subject of future work.

In comparison to the reference microstructures of the specimens in Fig. 3a and e recorded in the unloaded condition before testing, the micrographs taken in the loaded condition point out increasing topography changes along each GB upon the stepwise increase of the applied compressive strain to -6 %. Although the topography evolution is less pronounced than in the vicinity of the triple junction (cf. Fig. 1), accommodation of transformation incompatibilities by GBs is also necessary in bamboo-like microstructures, even in the bi-crystal with the low $\Delta\varepsilon_{theo}$ (Fig. 2a and Fig. 3 a - d). The associated transformation-induced stress concentrations trigger additional transformation events, i.e. the evolution of multiple martensite variants/plates in the individual grains of both bi-crystals. This is most prominent near the GBs indicated by the dashed ovals in Fig. 3c and g. In comparison to the relatively simple transformation path of Co-Ni-Ga single crystals, featuring single-variant SIMT under uniaxial loading [7,41], this more complex martensite morphology in direct vicinity of GBs in bamboo-like microstructures is in excellent agreement with observations in Ref. [24].

Fig. 4 illustrates the results of the *post mortem* OM and SEM analysis conducted after unloading from the maximum strain level of -6 %. Despite the obvious topography changes upon loading, the overview optical micrographs in Fig. 4a and d depict no kind of structural degradation in the unloaded state. The in-depth study via SEM (Fig. 4b,c and e,f) confirms the observations made by OM, i.e. GBs without any crack formed and covered with precipitates of the ductile γ-phase are present. Please note that the inferior kikuchi pattern quality along the GB in the IQ map of Fig. 4c most probably results from pronounced plastic deformation of the γ-phase instead of crack formation. This is also evidenced by the corresponding image obtained using the Argus detector shown in Fig. 4b, which reveals an intact GB.

The effect of bamboo grain structures on the functional properties and structural degradation in SMAs was investigated in a few studies focusing predominantly on Fe- and Cu-based systems [26,29,34]. In their study focusing on the damage evolution in micron-sized Cu-Zn-Al SMA wires, Ueland and Schuh [24] demonstrated excellent damage tolerance, i.e. resistance against GB cracking, for GBs perpendicular to the loading direction. The present results for the Co-Ni-Ga system are perfectly in line with those findings. Vollmer et al. [19] demonstrated for a bamboo-like Co-Ni-Ga specimen with a low $\Delta\varepsilon_{theo}$ excellent pseudoelastic properties, as no kind of degradation, i.e. neither structural nor functional, was observed. The bi-crystal characterized by the low $\Delta\varepsilon_{theo}$ of 0.2 % (Fig. 2a) demonstrates the same excellent resistance against GB cracking. Due to the low $\Delta\varepsilon_{theo}$ and the almost simultaneous onset of the SIMT in the ⟨105⟩- and ⟨314⟩-oriented grains (Fig. 3b) only moderate strain incompatibilities have to be accommodated at the GB. Unexpectedly, functional degradation in terms of evolution of irreversible strain is observed. In contrast to the solution-annealed and precipitate-free specimen in Ref. [19], in the current work ductile γ-phase precipitated along the GBs as well as in the interior of the grain.

On the one hand, it is supposed that the γ-phase precipitation is the main reason responsible for the accumulation of irreversible strains in all specimens of the present study. On the other hand, γ-phase precipitation is crucially needed to protect the GB against premature failure when considering any arbitrary kind of GB arrangement. Thus, in light of future application of polycrystalline Co-Ni-Ga conditions only samples containing γ-phase were considered here. Since the martensitic transformation is effectively constrained at the GBs, the stress-strain curves feature a more or less pronounced strain-hardening. Consequently, the stepwise increase of the applied compressive strain causes a progressive plastic deformation of the γ-phase. Furthermore, martensite plates are stabilized by dislocations in the vicinity of these heavily deformed γ-particles as evidenced by the IQ maps in Fig. 1, Fig. 4, Fig. 5 and Fig. 6. This mechanically stabilized martensite additionally contributes to the functional degradation.

To the best of the authors' knowledge, the current work explicitly details for the first time the impact of GB misorientation in Co-Ni-Ga bamboo-like microstructures, expressed by the amount of $\Delta\varepsilon_{theo}$ between two neighboring grains. Despite the well-known deteriorating features as detailed in [8], grain boundary engineering via precipitation of the γ-phase was performed in order to improve the structural integrity during pseudoelastic transformation, especially, in bi-crystals with high $\Delta\varepsilon_{theo}$ values (Fig 2b, Fig. 5 and Fig. 6). It is important to note that solution-annealed bi-crystals (not shown) equivalent to the specimen presented in Fig. 2b, i.e. featuring a bamboo grain structure as well as high $\Delta\varepsilon_{theo}$, showed instantaneous failure subsequently after cooling from the solution-annealing temperature to ambient temperature without an intermediate heat treatment step at 900°C. Differential scanning calorimetry (DSC) measurements (not shown) of the solution-annealed condition revealed a martensite start (M_s) temperature of about 30°C. Following cooling from the high-temperature regime transformation

incompatibilities arise from the thermally induced martensitic transformation causing an abrupt cracking of the GB. Consequently, the present results are a clear evidence for the effectiveness of grain boundary engineering in SMA systems featuring pronounced brittleness, e.g. Co-Ni-Ga or Fe-base alloys [23]. Although the bamboo grain structure presented in Fig. 2b features a distinctive transformation anisotropy, i.e. a high $\Delta\varepsilon_{theo}$ of 2.4 % and a sequential SIMT (Fig. 3f), extensive plastic deformation of the γ-precipitates is capable to accommodate the pronounced transformation strain incompatibilities. The complex multi-variant martensite morphology in the vicinity of the GB (Fig. 3g) additionally helps to accommodate the geometrical incompatibilities at the GB and prevents GB cracking. According to this, even critical bamboo-like microstructures with high $\Delta\varepsilon_{theo}$ feature excellent damage tolerance, however, only under the premise of grain boundary engineering via ductile second phases. The investigation of the functional properties and degradation under cyclic loading conditions will be subject of future work. It has to be clarified, if such critical bamboo structures demonstrate superior performance reported for bamboo structures so far [19,26,29,34].

Irregularly shaped grain boundary in a bamboo structure

Fig. 5 shows the characteristic stress-strain response and representative optical micrographs recorded at the specific positions (a) – (c) under loading for a bi-crystalline specimen featuring a GB not being perpendicular or parallel to the loading direction. The investigated bi-crystal features an identical pair of grain orientations as the bi-crystal shown in Fig. 2b, i.e. a pairing with ⟨115⟩ and ⟨112⟩ crystallographic orientations. However, instead of the related to the loading axis nearly perpendicular GB half of the present GB is inclined by about 45° as can be deduced from the orientation map in the inset of Fig. 5. Some aspects of the martensitic

transformation and the functional properties are similar to the results observed in Fig. 2b and Fig. 3e - h. Due to the aforementioned orientation dependence of σ_{crit} [39,40], again, a two-stage transformation behavior is visible in the stress-strain curve which can be seen in the optical micrograph in Fig. 5a. A large martensite plate evolves in the ⟨115⟩-oriented grain as a consequence of the significantly lower σ_{crit} of the ⟨115⟩ crystallographic orientation as compared to the ⟨112⟩ orientation [39]. In addition, functional degradation in terms of an accumulation of irreversible strains and a continuous decrease of σ_{crit} with increasing number of cycles takes place. The underlying microstructural mechanisms are pronounced plastic deformation of the ductile γ-phase and mechanically stabilized martensite in the vicinity of these heavily deformed particles as described above as well as illustrated for the present specimen by the optical micrograph in Fig. 5c and the IQ map in Fig. 5d, respectively. The stabilized martensite plates are nucleation spots and, consequently, promote further SIMT. Substantial crack formation detailed hereafter (in the context of structural degradation) additionally contributes to the accumulation of irreversible strains.

The aforementioned results demonstrate excellent resistance against GB cracking for bi-crystals with almost perfect bamboo-like GBs, i.e. GBs being almost straight. As can be deduced from the *in situ* OM study in Fig. 5 the shape of the GB, however, is another key criterion to be considered for high damage tolerance in envisaged applications. The micrograph in Fig. 5b illustrates premature crack formation at the inflection point of the GB after straining to -2.5 %. Upon further loading to -4 % (Fig. 5c) crack advance of the two previously formed cracks as well as further crack formation occurs in the vicinity of the GB inflection point. In comparison to the bamboo grain structure in Fig. 2b, the bi-crystal in Fig. 5 features the same pronounced transformation anisotropy, i.e. a high $\Delta\varepsilon_{theo}$ of 2.4 % and a sequential SIMT due to orientation

dependent differences of σ_{crit}. However, for the specimen condition characterized in Fig. 5 the grain boundary phase engineering is not capable to prevent premature failure anymore. The GB inflection point represents a microstructural notch. The stress concentrations resulting from both, transformation incompatibilities at the GB as well as the microstructural notch effect, exceed the capability of the ductile γ-phase to relieve the local stress peaks by pronounced plastic deformation sufficiently.

The *post mortem* EBSD analysis clarifies the prevailing fracture mechanisms. As it is well known from literature, intergranular fracture is the dominant failure mechanism in brittle single-phase polycrystalline SMA systems [4,20]. However, the IQ map in Fig. 5d reveals both, intergranular as well as transgranular fracture. The morphology of the γ-phase in Fig 5d has to be considered at this point. Instead of an intended thin continuous layer of the ductile second phase along the GB, a blocky morphology of the γ-precipitates was established. Most probably, in the present case crack nucleation starts at a GB segment not being decorated by the ductile γ-phase. However, further crack propagation along the GB is impeded by a ductile γ-precipitate in front of the crack tip forming a plastic zone and effectively to eventually increase the energy barrier for crack propagation. Such a crack growth behavior is in excellent agreement with the study of Dar et al. [20] in which the grain boundary phase engineering approach was introduced for several brittle SMAs. Once crack propagation along the GB is stopped, fracture proceeds in the interior of the grains, i.e. transgranular cracking is seen. These correlations could be observed for cracks forming at the triple junction as well (Fig. 1d).

Columnar grain structure

The characteristic stress-strain response of a bi-crystalline specimen with a GB parallel to the loading axis and the corresponding representative micrographs taken at positions (a) – (d) are shown in Fig. 6. In contrast to the aforementioned bi-crystals with bamboo-like microstructures, the EBSD orientation map (inset in Fig. 6) reveals the columnar grain structure. An ordinary high-angle GB separates two grains with ⟨115⟩ and ⟨213⟩ crystallographic orientation with respect to the loading axis featuring maximum theoretical transformation strains of about -4.2 % and -3.6 %, respectively [17]. Consequently, the grain structure features a $\Delta\varepsilon_{theo}$ of 0.6 %.

The stress-strain curve in Fig. 6 demonstrates continuous strain-hardening upon increasing deformation. Due to the similar resistance to the SIMT of the two crystallographic orientations [39,40] martensite plates are formed in both grains already at the very beginning of the martensitic transformation as evidenced by the micrograph at -1.5 % strain presented in Fig. 6a and, thus, no two-stage transformation is distinguishable. The complex martensite morphology with numerous interfaces results from the effectively constrained transformation at the GB. These transformation incompatibilities are highlighted by the pronounced topography changes along the parallel oriented GB upon straining during the IST (Fig. 6b). In addition, due to an incomplete back transformation of the stress-induced martensite pronounced functional degradation can be seen in the stress-strain response. After unloading from the maximum applied strain level of -6 % the corresponding micrograph in Fig. 6c still features significant topography. Since this columnar grained bi-crystal is characterized by a slightly lower value of σ_{crit}, i.e. lower transformation temperatures compared to the other specimens, the martensite plates are at least partly thermally stabilized due to testing at ambient temperature, and not fully mechanically stabilized by dislocations as observed in the vicinity of the deformed γ-particles. This issue may be attributed to sample to sample variations already observed in tests using Co-

Ni-Ga single crystals [38]. However, by heating from ambient temperature to 100°C shape recovery from -3.5 % to about -1 % takes place due to back transformation of the thermally stabilized martensite. This back transformation can be deduced by the topography changes between the micrographs in Fig. 6c and d recorded before and after heating, respectively. The degree of the remaining irreversible strains following the heating procedure is in accordance with the other specimens. Again, progressive plastic deformation of the ductile γ-phase and mechanically stabilized martensite mainly contribute to the functional degradation.

Despite the transformation incompatibilities and the concomitant topography evolution the columnar grain bi-crystal demonstrates the same excellent damage tolerance as bamboo grain structures with GB almost exclusively oriented perpendicular to loading direction. The overview optical micrographs in Fig. 6c and d of the finally unloaded state as well as the *post mortem* in-depth study via SEM presented in Fig. 6e and f reveal no traces of crack formation. In addition to this, Fig. 6 reveals that the GB is decorated by a continuous precipitation of the γ-phase, which is an obvious difference to the other sample conditions. The precipitation of secondary phases at GBs should in general be attributed to the GB energy [42]. However, GBs investigated in this study are of the same character. Thus, future work is crucially needed in order to analyse precipitations kinetics. The grain boundary phase engineering approach and the complex martensite morphology are capable to protect the GB against intergranular fracture. These findings are in excellent agreement with the results reported by Liu et al. [36,37] about columnar-grained microstructures in a Cu-Al-Mn SMA. Such microstructures fabricated by continuous unidirectional solidification possess a strong ⟨001⟩ texture along the solidification direction and straight low-energy GBs. Their excellent functional and structural properties were attributed to an improvement of the transformation compatibility and an avoidance of significant

stress concentrations. The present study, for the first time, extends these findings to columnar grained microstructures in SMAs separated by high-angle GBs in between grains with higher $\Delta\varepsilon_{theo}$.

Conclusions

The present work revealed the effect of grain boundary engineering on structural degradation of a Co-Ni-Ga high-temperature shape memory alloy. Incremental strain tests were conducted at ambient temperature for different oligocrystals. An *in situ* optical microscopy study and *post mortem* scanning electron microscopy analysis revealed microstructural characteristics causing structural as well as functional degradation during pseudoelastic loading. The major findings can be summarized as follows:

(1) Owing to the highly anisotropic transformation behavior geometrical incompatibilities and associated stress concentrations at GB triple junctions lead to premature failure.

(2) Bamboo grain structures with perpendicular oriented GBs in respect to the loading direction demonstrated excellent damage tolerance against GB cracking, however, only under the premise of grain boundary engineering via ductile second phases. Plastic deformation of the γ-phase is essential to accommodate pronounced transformation incompatibilities between unfavorable oriented grains.

(3) The shape of a GB in bamboo-like grain structures is a key criterion for structural degradation. In contrast to a straight GB, an inflection point represents a microstructural notch causing a stress peaks and premature cracking. Columnar grain structures feature excellent damage tolerance.

Acknowledgements

Financial support by Deutsche Forschungsgemeinschaft (DFG) within the Research Unit Program “Hochtemperatur-Formgedächtnislegierungen” (Project no. 200999873; Contract no. NI1327/3-2) is gratefully acknowledged. The work of Y.I.C. was carried out with financial support from the Ministry of Science and Education of Russian Federation (State Task no. 16.6554.2017/6.7). The authors acknowledge the assistance of Thomas Pham and Michael Wiegand with the experiments.

References

[1] D.C. Lagoudas: Shape Memory Alloys, Springer US, Boston, MA, 2008.
[2] K. Otsuka, C. M. Wayman (Eds.): Shape memory materials, 1st ed., Cambridge Univ. Press, Cambridge, 1999.
[3] G.S. Firstov, J. van Humbeeck, Y.N. Koval: High-temperature shape memory alloys, Mater. Sci. Eng., A 378 (2004) 2–10.
[4] J. Ma, I. Karaman, R.D. Noebe: High temperature shape memory alloys, Int. Mater. Rev. 55 (2013) 257–315.
[5] P.J.S. Buenconsejo, H.Y. Kim, S. Miyazaki: Effect of ternary alloying elements on the shape memory behavior of Ti–Ta alloys, Acta Mater. 57 (2009) 2509–2515.
[6] H. Sehitoglu, L. Patriarca, Y. Wu: Shape memory strains and temperatures in the extreme, Curr. Opin. Solid State Mater. Sci. 21 (2017) 113–120.
[7] A. Reul, C. Lauhoff, P. Krooß, M.J. Gutmann, P.M. Kadletz, Y.I. Chumlyakov, T. Niendorf et al.: In Situ Neutron Diffraction Analyzing Stress-Induced Phase Transformation and Martensite Elasticity in [001]-Oriented Co49Ni21Ga30 Shape Memory Alloy Single Crystals, Shap. Mem. Superelasticity 4 (2018) 61–69.
[8] E. Dogan, I. Karaman, Y.I. Chumlyakov, Z.P. Luo: Microstructure and martensitic transformation characteristics of CoNiGa high temperature shape memory alloys, Acta Mater. 59 (2011) 1168–1183.
[9] P.J. Brown, K. Ishida, R. Kainuma, T. Kanomata, K.-U. Neumann, K. Oikawa, B. Ouladdiaf et al.: Crystal structures and phase transitions in ferromagnetic shape memory alloys based on Co–Ni–Al and Co–Ni–Ga, J. Phys.: Condens. Matter 17 (2005) 1301–1310.
[10] J. Liu, H. Xie, Y. Huo, H. Zheng, J. Li: Microstructure evolution in CoNiGa shape memory alloys, J. Alloys Compd. 420 (2006) 145–157.
[11] J. Dadda, H.J. Maier, I. Karaman, H.E. Karaca, Y.I. Chumlyakov: Pseudoelasticity at elevated temperatures in [001] oriented Co49Ni21Ga30 single crystals under compression, Scr. Mater. 55 (2006) 663–666.
[12] J.A. Monroe, I. Karaman, H.E. Karaca, Y.I. Chumlyakov, H.J. Maier: High-temperature superelasticity and competing microstructural mechanisms in Co49Ni21Ga30 shape memory alloy single crystals under tension, Scr. Mater. 62 (2010) 368–371.

[13] I.V. Kireeva, C. Picornell, J. Pons, I.V. Kretinina, Y.I. Chumlyakov, E. Cesari: Effect of oriented γ′ precipitates on shape memory effect and superelasticity in Co–Ni–Ga single crystals, Acta Mater. 68 (2014) 127–139.
[14] I.V. Kireeva, J. Pons, C. Picornell, Y.I. Chumlyakov, E. Cesari, I.V. Kretinina: Influence of γ′ nanometric particles on martensitic transformation and twinning structure of L10 martensite in Co–Ni–Ga ferromagnetic shape memory single crystals, Intermetallics 35 (2013) 60–66.
[15] T. Niendorf, J. Dadda, J. Lackmann, J.A. Monroe, I. Karaman, E. Panchenko, H.E. Karaca et al.: Tension - Compression Asymmetry in $Co_{49}Ni_{21}Ga_{30}$ High-Temperature Shape Memory Alloy Single Crystals, Mater. Sci. Forum 738-739 (2013) 82–86.
[16] P. Krooß, T. Niendorf, P.M. Kadletz, C. Somsen, M.J. Gutmann, Y.I. Chumlyakov, W.W. Schmahl et al.: Functional Fatigue and Tension–Compression Asymmetry in [001]-Oriented Co49Ni21Ga30 High-Temperature Shape Memory Alloy Single Crystals, Shap. Mem. Superelasticity 1 (2015) 6–17.
[17] J. Dadda, H.J. Maier, D. Niklasch, I. Karaman, H.E. Karaca, Y.I. Chumlyakov: Pseudoelasticity and Cyclic Stability in Co49Ni21Ga30 Shape-Memory Alloy Single Crystals at Ambient Temperature, Metall and Mat Trans A 39 (2008) 2026–2039.
[18] P. Krooß, P.M. Kadletz, C. Somsen, M.J. Gutmann, Y.I. Chumlyakov, W.W. Schmahl, H.J. Maier et al.: Cyclic Degradation of Co49Ni21Ga30 High-Temperature Shape Memory Alloy, Shap. Mem. Superelasticity 2 (2016) 37–49.
[19] M. Vollmer, P. Krooß, C. Segel, A. Weidner, A. Paulsen, J. Frenzel, M. Schaper et al.: Damage evolution in pseudoelastic polycrystalline Co–Ni–Ga high-temperature shape memory alloys, J. Alloys Compd. 633 (2015) 288–295.
[20] R.D. Dar, H. Yan, Y. Chen: Grain boundary engineering of Co–Ni–Al, Cu–Zn–Al, and Cu–Al–Ni shape memory alloys by intergranular precipitation of a ductile solid solution phase, Scr. Mater. 115 (2016) 113–117.
[21] K. Ishida, R. Kainuma, N. Ueno, T. Nishizawa: Ductility enhancement in NiAl (B2)-base alloys by microstructural control, Metall. Trans. A 22 (1991) 441–446.
[22] R. Kainuma, K. Ishida, T. Nishizawa: Thermoelastic martensite and shape memory effect in B2 Base Ni-Al-Fe alloy with enhanced ductility, Metall. Trans. A 23 (1992) 1147–1153.
[23] M. Vollmer, C. Segel, P. Krooß, J. Günther, L.W. Tseng, I. Karaman, A. Weidner et al.: On the effect of gamma phase formation on the pseudoelastic performance of polycrystalline Fe–Mn–Al–Ni shape memory alloys, Scr. Mater. 108 (2015) 23–26.
[24] S.M. Ueland, C.A. Schuh: Grain boundary and triple junction constraints during martensitic transformation in shape memory alloys, J. Appl. Phys. 114 (2013) 53503.
[25] S.M. Ueland, C.A. Schuh: Superelasticity and fatigue in oligocrystalline shape memory alloy microwires, Acta Mater. 60 (2012) 282–292.
[26] S.M. Ueland, Y. Chen, C.A. Schuh: Oligocrystalline Shape Memory Alloys, Adv. Funct. Mater. 22 (2012) 2094–2099.
[27] T. Kusama, T. Omori, T. Saito, S. Kise, T. Tanaka, Y. Araki, R. Kainuma: Ultra-large single crystals by abnormal grain growth, Nat. Commun. 8 (2017) 354.
[28] T. Omori, T. Kusama, S. Kawata, I. Ohnuma, Y. Sutou, Y. Araki, K. Ishida et al.: Abnormal grain growth induced by cyclic heat treatment, Science 341 (2013) 1500–1502.

[29] Y. Sutou, T. Omori, K. Yamauchi, N. Ono, R. Kainuma, K. Ishida: Effect of grain size and texture on pseudoelasticity in Cu–Al–Mn-based shape memory wire, Acta Mater. 53 (2005) 4121–4133.
[30] Y. Sutou, T. Omori, J.J. Wang, R. Kainuma, K. Ishida: Effect of grain size and texture on superelasticity of Cu-AI-Mn-based shape memory alloys, J. Phys. IV France 112 (2003) 511–514.
[31] Y. Sutou, T. Omori, R. Kainuma, K. Ishida: Grain size dependence of pseudoelasticity in polycrystalline Cu–Al–Mn-based shape memory sheets, Acta Mater. 61 (2013) 3842–3850.
[32] T. Omori, K. Ando, M. Okano, X. Xu, Y. Tanaka, I. Ohnuma, R. Kainuma et al.: Superelastic effect in polycrystalline ferrous alloys, Science 333 (2011) 68–71.
[33] T. Omori, H. Iwaizako, R. Kainuma: Abnormal grain growth induced by cyclic heat treatment in Fe-Mn-Al-Ni superelastic alloy, Mater. Des. 101 (2016) 263–269.
[34] T. Omori, M. Okano, R. Kainuma: Effect of grain size on superelasticity in Fe-Mn-Al-Ni shape memory alloy wire, APL Mater. 1 (2013) 32103.
[35] M. Vollmer, P. Krooß, I. Karaman, T. Niendorf: On the effect of titanium on quenching sensitivity and pseudoelastic response in Fe-Mn-Al-Ni-base shape memory alloy, Scr. Mater. 126 (2017) 20–23.
[36] J.-L. Liu, H.-Y. Huang, J.-X. Xie: The roles of grain orientation and grain boundary characteristics in the enhanced superelasticity of Cu71.8Al17.8Mn10.4 shape memory alloys, Mater. Des. 64 (2014) 427–433.
[37] J.-L. Liu, H.-Y. Huang, J.-X. Xie, S. Xu, F. Li: Superelastic fatigue of columnar-grained Cu-Al-Mn shape memory alloy under cyclic tension at high strain, Scr. Mater. 136 (2017) 106–110.
[38] T. Niendorf, P. Krooß, C. Somsen, G. Eggeler, Y.I. Chumlyakov, H.J. Maier: Martensite aging – Avenue to new high temperature shape memory alloys, Acta Mater. 89 (2015) 298–304.
[39] Y. Chumlyakov, E. Panchenko, I. Kireeva, I. Karaman, H. Sehitoglu, H.J. Maier, A. Tverdokhlebova et al.: Orientation dependence and tension/compression asymmetry of shape memory effect and superelasticity in ferromagnetic Co40Ni33Al27, Co49Ni21Ga30 and Ni54Fe19Ga27 single crystals, Mater. Sci. Eng., A 481-482 (2008) 95–100.
[40] J. Dadda: Thermomechanical and Microstructural Characterization of Co49Ni21Ga30 and Co38Ni33Al29 High-temperature Shape Memory Alloy Single Crystals, Paderborn, Univ., Thesis (2009).
[41] J. Dadda, H. J-rgen Maier, I. Karaman, Y. Chumlyakov: High-temperature in-situ microscopy during stress-induced phase transformations in Co 49 Ni 21 Ga 30 shape memory alloy single crystals, Int. J. Mater. Res. 101 (2010) 1–11.
[42] T. Omori, S. Abe, Y. Tanaka, D.Y. Lee, K. Ishida, R. Kainuma: Thermoelastic martensitic transformation and superelasticity in Fe–Ni–Co–Al–Nb–B polycrystalline alloy, Scr. Mater. 69 (2013) 812–815.

Table 1

Grain boundary morphology	Crystal orientations	Max. theoretical transformation strains	Max. transformation strain difference $\Delta\varepsilon_{theo}$
Triple junction (Fig. 1)	⟨115⟩ | ⟨103⟩ | ⟨112⟩	-4.2 % | -4.2 % | -1.8 %	2.4 %
Bamboo (Fig. 2a)	⟨105⟩ | ⟨314⟩	-4.2 % | -4.0 %	0.2 %
Bamboo (Fig. 2b)	⟨112⟩ | ⟨115⟩	-1.8 % | -4.2 %	2.4 %
Irregular shaped bamboo (Fig. 5)	⟨112⟩ | ⟨115⟩	-1.8 % | -4.2 %	2.4 %
Columnar (Fig. 6)	⟨213⟩ | ⟨115⟩	-3.6 % | -4.2 %	0.6 %

Table 1: Characteristics of the investigated specimens, i.e. grain boundary morphology, crystal orientations with respect to the loading direction, max. theoretical transformation strains ε_{tr} and max. transformation strain difference $\Delta\varepsilon_{theo}$.

Fig. 1

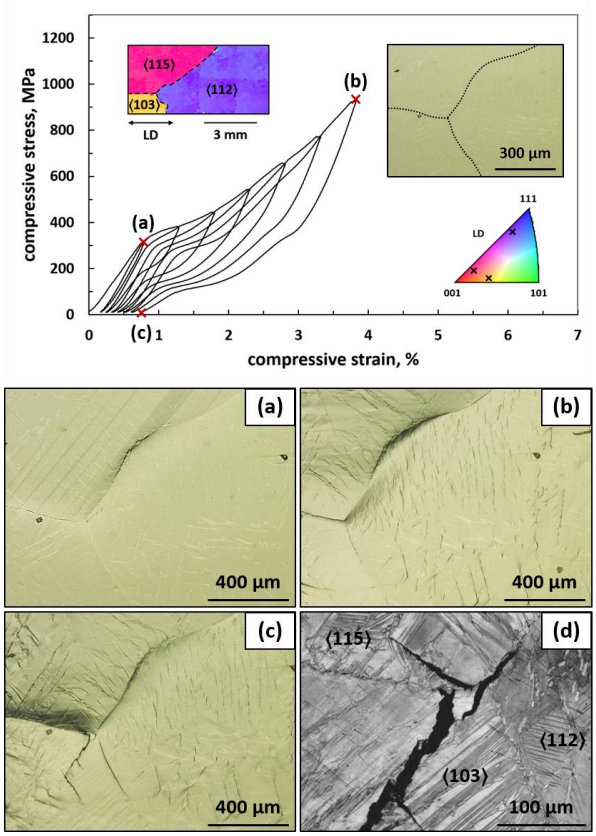

Figure 1: Characteristic stress-strain curve at ambient temperature for a tri-crystalline Co-Ni-Ga specimen. The evolution of surface topography and crack formation is illustrated by in situ optical micrographs at specific points of the stress-strain curve marked with (a) – (c). A post mortem EBSD image quality (IQ) map of the crack area is shown in (d). An EBSD orientation map of the specimen, the color coded standard triangle (lower right hand side) and the reference microstructure (upper right hand side) before pseudoelastic testing are presented as insets in the stress-strain diagram. Loading direction is parallel to the horizontal direction.

Fig. 2

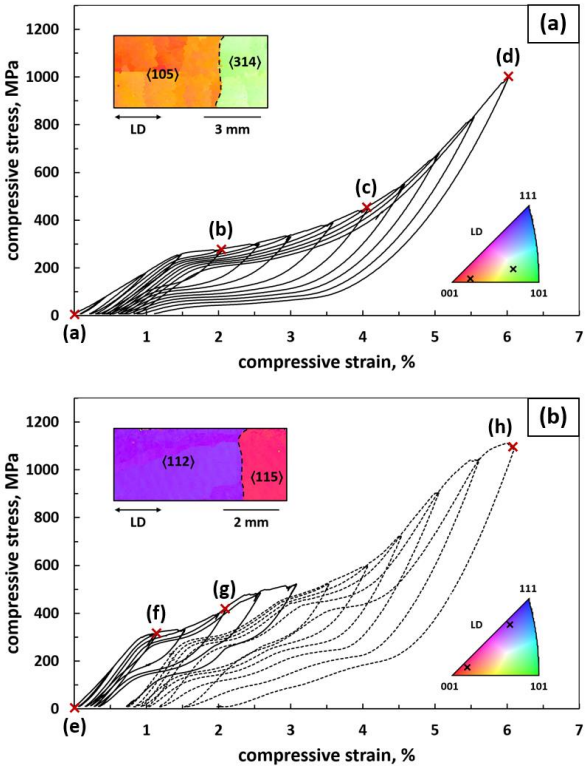

<u>Figure 2:</u> Characteristic stress-strain curves at ambient temperature for bi-crystalline Co-Ni-Ga specimens featuring a bamboo-like microstructure with low (a) and high (b) transformation strain difference (see main text for details). EBSD orientation maps of the specimens and the color coded standard triangle are presented as insets in the stress-strain diagrams. Loading direction is parallel to the longer specimen axes, i.e. horizontal.

Fig. 3

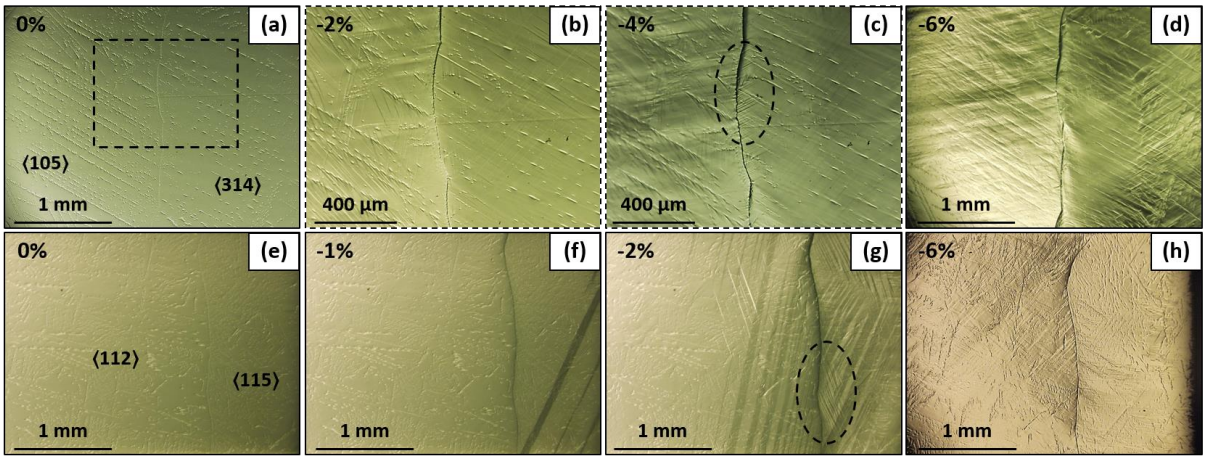

Figure 3: In situ OM analysis under compressive load at ambient temperature of the bamboo-like bi-crystalline Co-Ni-Ga specimens featuring low (a - d) and high (e - h) $\Delta\varepsilon_{theo}$*. Each micrograph was recorded under loading at specific strain values (marked as a - h) in the stress-strain curves in Fig. 2a and b. The dashed rectangle in (a) indicates the position of the micrographs (b) and (c). Loading direction is horizontal.*

Fig. 4

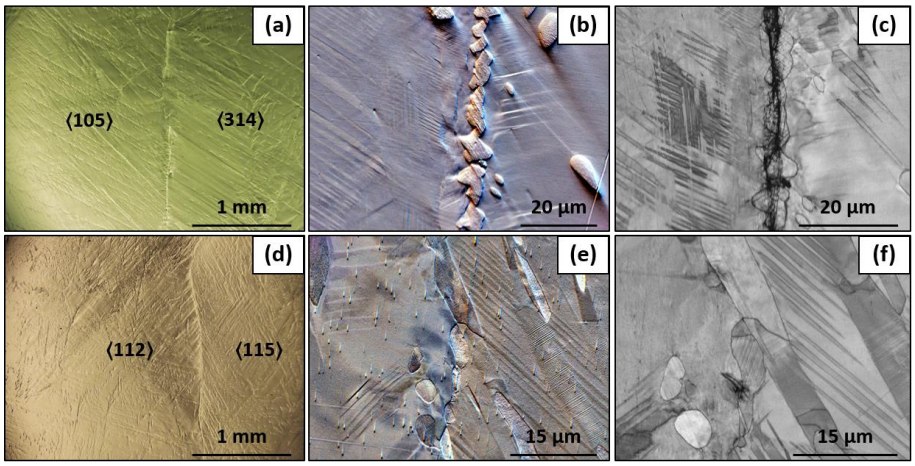

<u>Figure 4:</u> Post mortem OM and SEM analysis of the bamboo-like bi-crystalline Co-Ni-Ga specimens featuring low (a - c) and high (d - f) $\Delta\varepsilon_{theo}$*. Optical micrographs in (a) and (d) showing an overview of the GBs were recorded in unloaded state under the same conditions as applied in the in situ analysis shown in Fig. 3. Images of the Argus detector in (b) and (d) as well as EBSD IQ maps in (c) and (f) highlight details in the GB vicinities. See main text for details. Loading direction horizontal.*

Fig. 5

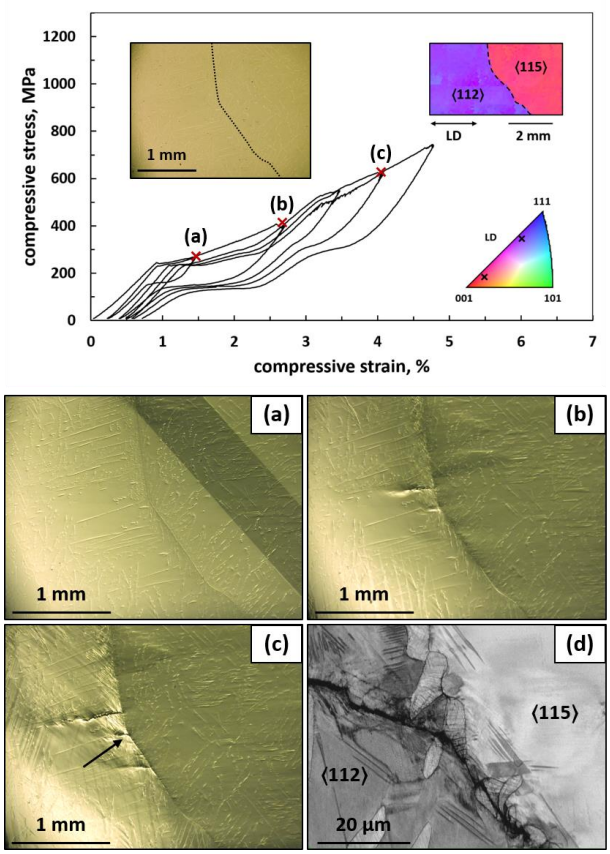

Figure 5: Characteristic stress-strain curve at ambient temperature for a bi-crystalline Co-Ni-Ga specimen with bamboo-like microstructure featuring an irregularly shaped grain boundary. The evolution of surface topography and crack formation is illustrated by in situ optical micrographs at specific points of the stress-strain curve marked with (a) – (c). A post mortem EBSD IQ map of a crack area marked by the black arrow in (c) is shown in (d) (please note the significantly different scale bars). An EBSD orientation map of the specimen, the color coded standard-triangle and the reference microstructure before pseudoelastic testing are presented as insets in the stress-strain diagram. Loading direction is horizontal.

Fig. 6

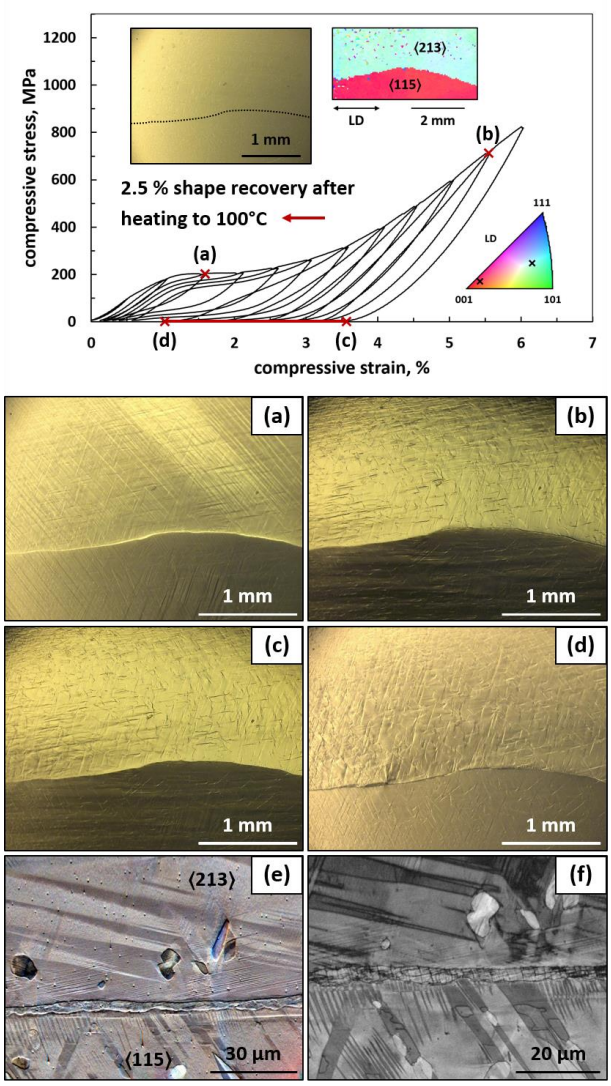

<u>Figure 6:</u> Characteristic stress-strain curve at ambient temperature for a bi-crystalline Co-Ni-Ga specimen with columnar grain structure. The evolution of surface topography is illustrated by in situ optical micrographs at specific points of the stress-strain curve marked with (a) – (d). A post mortem Argus detector image and EBSD IQ map of the crack free grain boundary are shown in (e) and (f), respectively. An EBSD orientation map of the specimen, the color coded standard-triangle and the reference microstructure before pseudoelastic testing are presented as insets in the stress-strain diagram. Loading direction is horizontal.

Autorenversion von: Lauhoff, C., Vollmer, M., Krooß, P. et al. Pathways Towards Grain Boundary Engineering for Improved Structural Performance in Polycrystalline Co–Ni–Ga Shape Memory Alloys. Shap. Mem. Superelasticity 5, 73–83 (2019). https://doi.org/10.1007/s40830-018-00204-3